Received: 5 February 2020 | Revised: 13 March 2020 | Accepted: 16 March 2020

DOI: 10.1002/ansa.202000002

ANALYTICAL SCIENCE ADVANCES

WILEY

FULL ARTICLE

Influence of core size and capping ligand of gold nanoparticles on the desorption/ionization efficiency of small biomolecules in AP-SALDI-MS

Zhen Liu[1] | **Peng Zhang**[2] | **Andrea Pyttlik**[3] | **Tobias Kraus**[3,4] | **Dietrich A. Volmer**[5]

[1]Institute of Bioanalytical Chemistry, Saarland University, Saarbrücken, Germany

[2]School of Materials Science and Engineering, Sun Yat-sen University, Guangzhou, China

[3]INM-Leibniz Institute for New Materials, Saarbrücken, Germany

[4]Institute of Colloid and Interface Chemistry, Saarland University, Saarbrücken, Germany

[5]Department of Chemistry, Humboldt-Universität zu Berlin, Berlin, Germany

Correspondence
Prof. Dr. Dietrich A. Volmer, Department of Chemistry, Humboldt-Universität zu Berlin, Brook-Taylor-Str. 2, 12489 Berlin, Germany
Email: dietrich.volmer@hu-berlin.de

Funding information
China Scholarship Council

Abstract

Gold nanoparticles (AuNP) are frequently used in surface-assisted laser desorption/ionization mass spectrometry (SALDI-MS) for analysis of biomolecules because they exhibit suitable thermal and chemical properties as well as strong surface plasmonic effects. Moreover, the structures of AuNP can be controlled by well-established synthesis protocols. This was important in the present work, which studied the influence of the nanoparticles' structures on atmospheric pressure (AP)-SALDI-MS performance. A series of AuNP with different core sizes and capping ligands were investigated, to examine the desorption/ionization efficiency (DIE) under AP-SALDI conditions. The results showed that both the AuNP core size as well as the nature of the surface ligand had a strong influence on DIE. DIE increased with the size of the AuNP and the hydrophobicity of the ligands. Chemical interactions between ligand and analytes also influenced DIE. Moreover, we discovered that removing the organic ligands from the deposited AuNP substrate layer by simple laser irradiation prior to LDI further amplified DIE values. The optimized AuNP were successfully used to analyze a wide arrange of different low molecular weight biomolecules as well as a crude pig brain extract, which readily demonstrated the ability of the technique to detect a wide range of lipid species within highly complex samples.

1 | INTRODUCTION

Since cobalt nanoparticles were first used for surface-assisted laser desorption/ionization mass spectrometry (SALDI-MS) by Tanaka *et al*,[1] nanomaterials made from carbon,[2–4] silicon,[5–7] metals (Au, Ag, Pa, etc.),[8–10] metal oxides,[11–13] and others materials[14–17] have been successfully applied to SALDI-MS. In general, nanoparticles are excellent substrate options for SALDI, because they require only simple and easy sample preparation techniques and the materials often exhibit minimal background signals – in particular in the low *m/z* range – as compared to matrix-assisted laser desorption/ionization (MALDI).[18–20] SALDI efficiencies can be enhanced by optimizing the nanoparticular structures, for example, by modifying the core size and nature of the surface ligands,[18] which was shown to be vital for sensitive quantitative analysis of biomolecules.[20]

In previous studies, it was found that desorption/ionization efficiency of SALDI was highly dependent on physical (size, surface roughness, light absorption, electrical conductivity, melting point, etc.) and chemical (surface modification, binding energy to analytes, etc.) properties of the nanomaterials.[18–23] Gold nanoparticles (AuNP) exhibit excellent electrical conductivities, thermal and chemical stabilities and strong light

absorption due to plasmonic effects. Furthermore, gold nanoparticles can be readily obtained using well-established synthesis protocols. Consequently, they have been frequently used for SALDI-MS analysis of biomolecules. Mclean *et al*[24] applied AuNP of different sizes (2-10 nm) to detect peptides. The authors found a size effect on desorption/ionization efficiency of peptides, where larger AuNP provided better performance. Ligand-free AuNP were reported by Amendola *et al*[25] that exhibited low background levels in the low mass range ($m/z < 500$) as compared to AuNP with surface-protected agents, providing picomolar level detection levels for small molecules such as arginine, fructose, atrazine, anthracene, and paclitaxel. Flower-like gold nanoparticles were used by Havel *et al* as mediators to enhance desorption/ionization of peptides.[26] The authors illustrated that the ion intensities for the peptides were up to 7.5-fold higher using gold nanoflowers as substrate as compared to α-cyanohydroxycinnamic acid (CHCA) as MALDI matrix. Using gold nanorods (AuNR), Castellana *et al* demonstrated that infrared laser desorption/ionization-MS was capable of analyzing peptides very efficiently.[27] Furthermore, fluorinated AuNP were prepared for comprehensive analysis of metabolites in biological tissues using nanostructure imaging mass spectrometry (NIMS) with minimal background noise levels and high sensitivity as illustrated by Palermo *et al*.[28] Only low laser energies were required during this process, which lead to very gentle desorption/ionization conditions with limited in-source fragmentation of the metabolites. Chiang *et al*[29] used mixed gold nanoparticles with diameters of 3 and 14 nm as probes for SALDI-MS to detect amino-thiol groups. The authors illustrated that larger size gold nanoparticles selectively captured amino-thiol on the surface, while the smaller particles improved sensitivity. Glutathione, cysteine, and homocysteine were successfully detected at detection limits of 2, 20, and 44 nM, respectively. Son *et al*[30] used citrate-capped AuNP with diameter of 12 nm to selectively detect triacylglycerols from crude lipid mixtures at very low levels, approximately 100-fold lower than by MALDI with dihydroxybenzoic acid (DHB) as matrix. Liu *et al*[31] utilized ultra-thin, homogenous $[AuNP]_n$ monolayer substrates for SALDI, which provided excellent signal intensities and low background for a wide range of analytes such as fatty acids, peptides, amino acids, saccharides, and drugs. AuNP were also used to directly analyze endogenous and exogenous compounds from latent fingerprint and image their distribution, without disturbing the fingerprint patterns, as demonstrated by Tang *et al*.[32]

While AuNP were shown to be well-suited functional substrates for SALDI-MS, the factors governing their performance are not yet fully understood. In this paper, various parameters of AuNP influencing desorption/ionization efficiency of analytes were systematically studied. Several different ligands for functionalized AuNP of different sizes, including oleyamine, alkanethiol, 11-mercaptoundecanoic acid, and 11-mercapto-1-undecanol, were investigated as substrates for AP-SALDI-MS. The performance of AuNP was initially evaluated by using linoleic acid as analyte, followed by an application to a wider range of low molecular weight molecules, such as fatty acids, amino acids, small peptides, saccharides, drugs, and phospholipids. The optimized substrate was then used for analysis of fatty acids and phospholipids in an extract of pig brain.

2 | MATERIALS AND METHODS

2.1 | Chemicals and reagents

Palmitic acid, stearic acid, oleic acid, linoleic acid, erythromycin A, aspartic acid, and phenylalanine were purchased from Sigma–Aldrich (Steinheim, Germany); D-fructose and D-lactose from Merck (Darmstadt, Germany); 1,2-dioleoyl-sn-glycero-3-phosphatidylcholines (PC 36:2), 1,2-dioleoyl-*sn*-glycero-3-phosphatidylethanolamine (PE 36:2), docosahexaenoic acid (DHA), eicosatetraenoic acid (EPA), timolol maleate, leu-enkephalin, and bradykinin from Cayman Chemicals (Hamburg, Germany); and acetonitrile (ACN) and methanol from VWR chemicals (Darmstadt, Germany). All chemicals were used without further pretreatment. Deionized water was generated by a Millipore (Bedford, MA, USA) water purification system.

Pig brains were purchased from a local market. Liquid extraction of the brains was performed according to a published protocol[33] and the extract stored at −32°C prior to SALDI-MS experiments.

AuNP with different core sizes, capping ligands, and dispersion solvents were prepared by using an adapted protocol by Zheng *et al*.[34] Briefly, oleyamine (OAm)-capped monodisperse AuNP were synthesized with an amine-borane complex as reducing agent. The nanoparticle sizes (radii, 1.2, 3.2, and 4.7 nm) were controlled by tuning the ratio of $HAuCl_4 \cdot 3H_2O$ and reducing agent as well as the reaction time.[35] Ligand exchange was performed to cap the AuNP with butanethiol (B), decanethiol (D), hexadecanethiol (H), 11-mercaptoundecanoic acid (MA), and 11-mercaptoundecanol (MO). The prepared nanoparticles were separated from the precursor solution and re-dispersed in methanol, hexane, and toluene, to achieve good colloidal stability. For clarity, AuNP were named using the nomenclature AuNP[X-*n*-Y], with X, *n*, and Y corresponding to capping ligand, core size, and dispersion solvent, respectively. For example, AuNP[B-1-H] represents AuNP with capping ligand of butanethiol, core radius of 1.2 nm, dispersed in hexane (all nanoparticles are summarized in Table 1). The stock solutions of AuNP were prepared at 1 mg/mL and used directly for SALDI-MS if not otherwise specified.

2.2 | Spectroscopic characterization of AuNP

X-ray scattering experiments were performed using a Xeuss 2.0 (Xenocs, Sassenage, France) instrument, equipped with a GeniX Low Divergence Cu-Kα source; the X-ray wavelength was 1.54 Å and the scattering signal was collected with a Dectris Pilatus 1 M detector; sample to detector

TABLE 1 Investigated gold nanoparticles and naming scheme[a] for particles

	Composition		
Name	Ligand	Core size (radius, nm)	Solvent
AuNP[B-1-H]	Butanethiol	1.2	Hexane
AuNP[D-1-H]	Decanethiol	1.2	Hexane
AuNP[H-1-H]	Hexadecanethiol	1.2	Hexane
AuNP[OAm-1-H]	Oleyamine	1.2	Toluene
AuNP[MA-1-M]	11-Mercaptoundecanoic acid	1.2	Methanol
AuNP[MO-1-M]	11-Mercaptoundecanol	1.2	Methanol
AuNP[D-3-H]	Decanethiol	3.2	Hexane
AuNP[OAm-3-H]	Oleyamine	3.2	Toluene
AuNP[H-4-H]	Hexadecanethiol	4.7	Hexane
AuNP[OAm-4-H]	Oleyamine	4.7	Toluene

[a] AuNP were named using the nomenclature AuNP[X-*n*-Y], with X, *n*, and Y corresponding to capping ligand, core size, and dispersion solvent, respectively.

distance was calibrated with silver behenate. UV/Vis characterization of AuNP samples was performed with a Jasco V-650 spectrophotometer (Jasco, Easton, MD, USA). The concentration of the AuNP solutions for UV/Vis measurements was 6 μg/mL.

2.3 | Preparation of SALDI samples

Stock solutions of analytes were prepared as follows: fatty acids (palmitic acid, stearic acid, oleic acid, linoleic acid, EPA, DHA, EPA) and drugs (erythromycin A, timolol maleate) were dissolved in methanol at 1 mM; amino acids (aspartic acid, phenylalanine), small peptides (leu-enkephalin, bradykinin) and saccharides (D-fructose, D-lactose) were dissolved in water at 10 mM. All stock solutions were stored at −20°C and diluted to the required concentration prior to use. If not otherwise specified, analyte solutions were diluted to 100 μM in methanol prior to the SALDI experiments. Sodium and potassium ions were added to analyte solutions if needed.

SALDI sample deposition was performed using the two-layer dried droplet method. Initially, 0.5 μL of AuNP solution was pipetted onto the steel target. After solvent evaporation, 0.5 μL of analyte solution was pipetted onto the AuNP and dried at ambient conditions.

2.4 | Mass spectrometry

MS experiments were performed with a Bruker (Bremen, Germany) Esquire HCT$^+$ 3D quadrupole ion trap mass spectrometer coupled with a MassTech (Burtonsville, MD, USA) atmospheric pressure-MALDI source. A Nd:YAG laser emitting at 355 nm was used as light source. If not otherwise mentioned, the laser energy was set to 50% and the repetition rate to 200 Hz. Full scan mass spectra were acquired in positive ion mode from *m/z* 50 to 1000 using a linear rastering motion of the target plate. Ion currents were accumulated as follows: rastering velocity, 40.0 mm/min; scan length, 2.0 mm; scan height, 2.0 mm; raster spacing, 0.5 mm; step size, 0.5 mm, raster direction, horizontal. A drying gas temperature of 50°C at a flow rate of 5.0 L/min was used.

3 | RESULTS AND DISCUSSION

The SALDI experiments shown in this work were performed utilizing an atmospheric pressure (AP) MALDI source, which enabled simple and rapid sample preparation as compared to vacuum-based ion sources, which was important for quick method optimization. The soft ionization conditions at atmospheric pressure and the resulting reduced or absent precursor ion fragmentation[36,37] generally provides ionization and transport efficiencies comparable to vacuum MALDI.[38,39]

It has been previously shown that certain properties of nanomaterials (size, ligands, concentration, etc.) play vital roles in the desorption/ionization efficiency (DIE) under vacuum SALDI conditions.[18-20] However, to our knowledge, no such investigation has been performed for AP-SALDI. In this study, we investigated AP-AuNP-assisted LDI of different sizes, carrying various organic ligands at different concentration levels, and their effect on DIE of selected analytes.

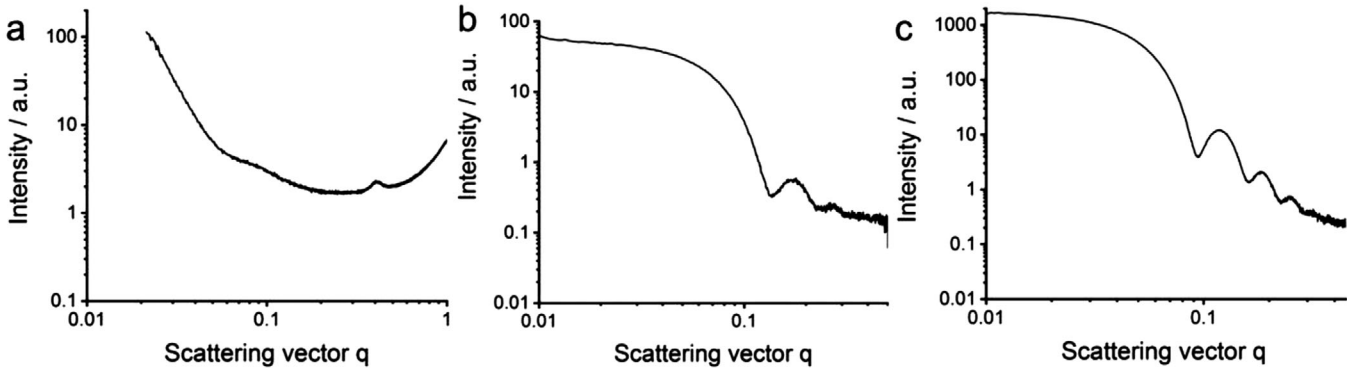

FIGURE 1 SAXS characterization of AuNP: A, 1.2 nm; B, 3.2 nm; and C, 4.7 nm

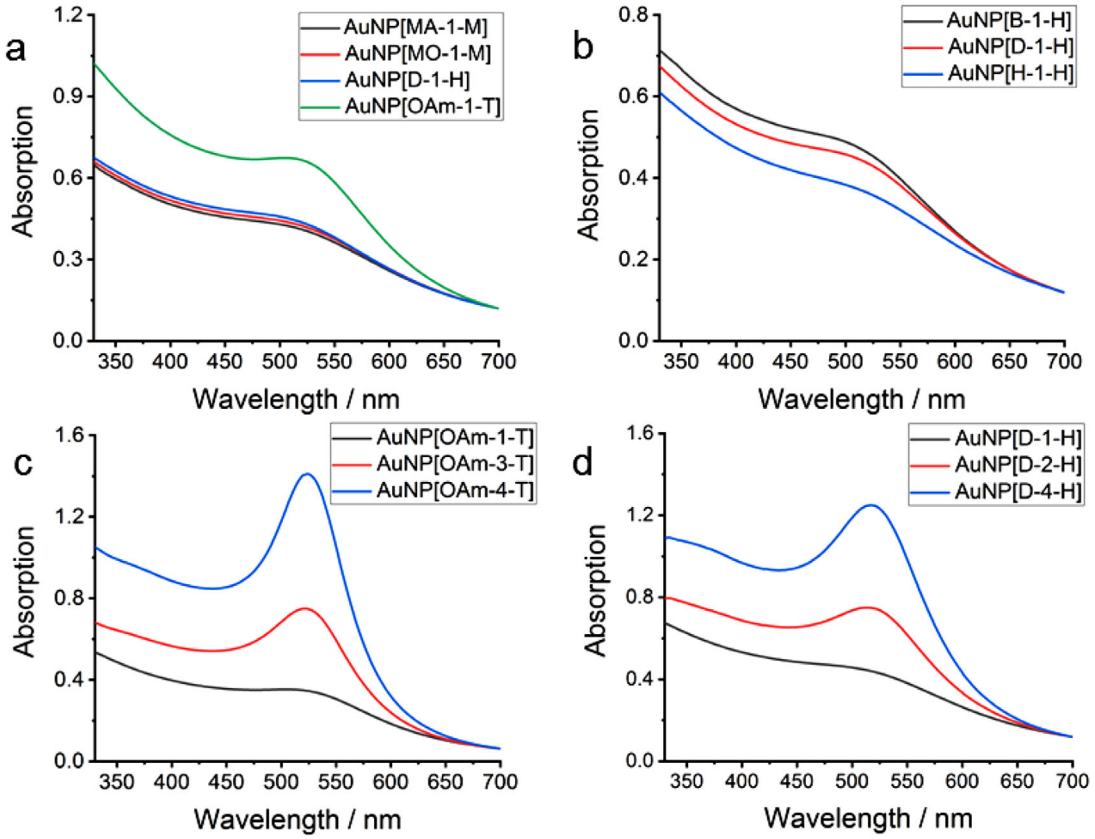

FIGURE 2 UV/Vis spectra of (A) 1.2 nm radius AuNP with different types of ligands, (B) 1.2 nm AuNP with alkanethiol ligand of different size, (C) AuNP with oleyamine as ligand for different core sizes, and (D) AuNP with alkanethiol as ligand for different core sizes. The concentrations of AuNP solutions for UV/Vis measurement were 6 μg mL^{-1}

3.1 | Initial characterization of the AuNP

Sizes of AuNP[OAm-H] were characterized by small angle X-ray scattering (SAXS) (Figure 1). After fitting, the radii of AuNP[OAm-H] were determined as 1.4, 3.2, and 4.7 nm, respectively. Other AuNP including AuNP[B-H], AuNP[D-H], AuNP[H-H], AuNP[MA-M], AuNP[MO-M], and AuNP[AT-H] were subsequently obtained via ligand exchange from the AuNP[OAm-H] nanoparticles (see Section 2).

The light absorption properties of these gold nanoparticles were measured by UV/Vis spectroscopy (Figure 2). AuNP[MA-1-M], AuNP[MO-1-M], and AuNP[D-1-H] did not exhibit distinct absorption maxima, but rather absorption plateaus at ~490 nm, while AuNP[OAm-1-H] absorbed with slightly higher intensity at 505 nm (Figure 2A). Similarly, AuNP[B-1-H], AuNP[D-1-H], and AuNP[H-1-H] exhibited plateau regions at ~490 nm (Figure 2B), which shifted to red and absorption decreased as the ligand length was increased. For AuNP[OAm-1-H], AuNP[OAm-3-H], and

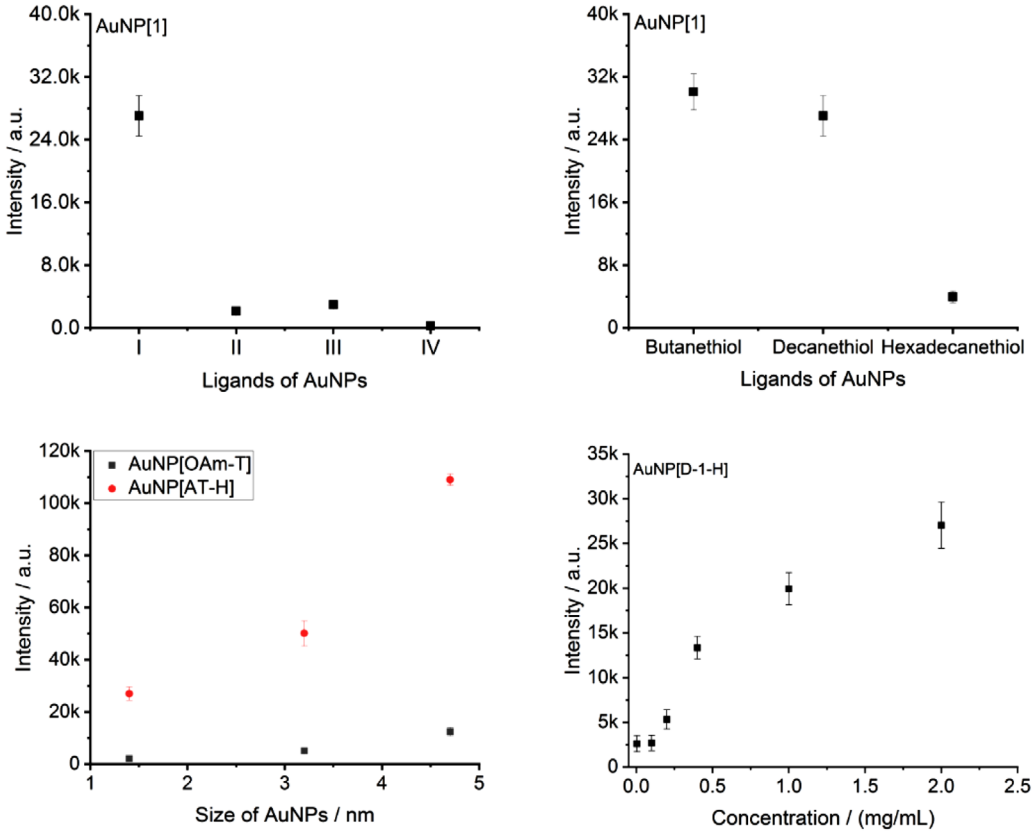

FIGURE 3 Different effects for AuNP on signal intensity of linoleic acid in SALDI-MS: (A) type of ligand, (B) ligand size, (C) core size and (D) AuNP concentration. I, II, III, and IV denote 1-decanethiol, oleyamine, 11-mercaptoundecanoic acid, and 11-mercapto-1-undecanol ligands, respectively

AuNP[OAm-4-H], absorption showed maxima at 505, 521, and 524 nm, respectively (Figure 2C). There was some red-shifting as the size of AuNP increased. Finally, AuNP[AT-1-H], AuNP[AT-3-H], and AuNP[AT-4-H] exhibited maxima at 490, 513, and 517 nm, respectively, with red-shifting and strong absorption increase as the size of AuNP increased (Figure 2D).

3.2 | Effects of ligand and nanoparticle properties on DIE

3.2.1 | Nature of the ligand

In this study, we compared different types of organic ligands for the AuNP to assess potential ligand effects on DIE in SALDI-MS, namely oleyamine, 11-mercaptoundecanoic acid, 11-mercapto-1-undecanol, and 1-decanethiol, all with identical radius of 1.2 nm. We chose linoleic acid as representative analyte in these experiments. As previously observed, salt adducts were common in the mass spectra and formed the base peaks in all experiments (for linoleic acid, these signals were at *m/z* 303 and 319, corresponding to $[M+Na]^+$ and $[M+K]^+$, respectively). We summed the ion currents of these two species and compared the four types of AuNP ligands. As shown in Figure 3A, the signal intensity for linoleic acid from AuNP[D-1-H] (= 1-decanethiol) was significantly higher than those obtained for the other three ligands, which is consistent with previous findings, showing that signal intensities from hydrophobic nanomaterials are higher than from hydrophilic nanomaterials.[28] This is related to higher local temperatures obtained with the hydrophobic nanomaterials and thus slower energy dispersion. However, surprisingly, analyte signals were much lower for the similarly hydrophobic oleyamine ligand, which is a weakly bound ligand in comparison to the covalently-bound thiol ligands. We hypothesize that this deviating behavior was due to excess amounts of oleyamine on the substrate surface. Stable AuNP-oleyamine dispersions required large amounts of oleyamine to keep the nanoparticles in solution (the concentration was approximately one order of magnitude higher than for the thiol-containing ligands as described in the Section 2; further details are given in the Supporting Information). This excess ligand material can interfere with the desorption/ionization by potentially forming a dense layer or bilayer on the surface of the AuNP, thus separating the analyte from the nanoparticles. A similar behavior was seen during SALDI-MS analysis of peptides using cetyltrimethylammonium bromide (CTAB)-capped gold nanorods (AuNR).[27] The authors of that study suggested that the presence of CTAB on the surface of the nanorods inhibited desorption/ionization

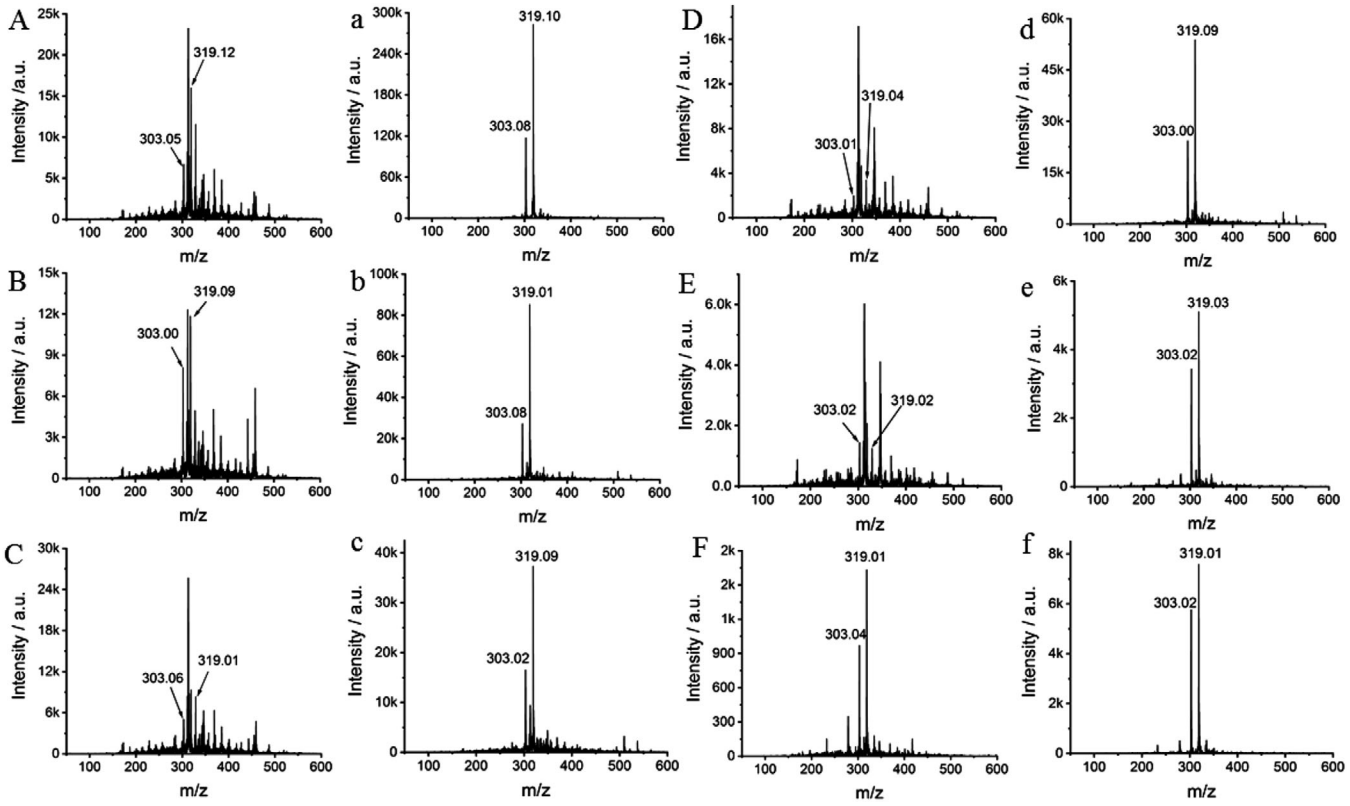

FIGURE 4 AuNP[D-1-H]-assisted LDI mass spectra of linoleic acid at different concentrations: (A, a) 2.0, (B, b) 1.0, (C, c) 0.4, (D, d) 0.2, (E, e) 0.1, (F, f) 0.04 mg/mL. Panels A-F show mass spectra of linoleic acid from ligand-capped AuNP; panels a-f, mass spectra of linoleic acid after initial laser irradiation of the AuNP surface. (Signals at *m/z* 303 and 319 correspond to $[M+Na]^+$ and $[M+K]^+$, respectively)

of analyte because CTAB did not provide a sufficient source for ionizing protons and because the positively-charged CTAB bilayer inhibited the analyte from adsorbing to the nanorod surface. We believe that the AuNP-oleyamine system is similarly restricted in comparison to the hydrophobic AuNP-decanethiol nanoparticles.

For AuNP[MA-1-M], the obtained signal intensities for linoleic acid were higher than for AuNP[MO-1-M], which can be explained by the ligand's chemical properties in comparison to linoleic acid, which were more similar for 11-mercaptoundecanoic acid than for 11-mercaptoundecanol, enabling closer interaction of analyte and AuNP for AuNP[MA-1-M] than for AuNP[MO-1-M], with resulting improved energy transfer.

From the above observations, we suggest that the chemical properties of the nanoparticle's ligands and the interaction of ligand with analyte are more important for efficient desorption/ionization than increased UV/Vis absorption (see previous section).

3.2.2 | Length of ligand

In the next set of experiments, the influence of the length of the carbon chain of the ligands on DIE was investigated using alkanethiol-capped AuNP of different lengths. In these experiments, butanethiol, decanethiol, and hexadecanethiol were compared as ligands. Figure 3B demonstrates that the signal intensity of linoleic acid decreased strongly with increasing size of the ligand, declining approximately 10-fold from AuNP[B-1-H] over AuNP[D-1-H] to AuNP[H-1-H]. This is likely related to thermal conductivity and UV/Vis absorption, which both decrease with increasing size of the ligand and thus give reduced energy transfer from the AuNP to linoleic acid.

3.2.3 | Ligand-capped versus ligand-free AuNP

Chemical-free AuNP have been shown to provide improved performance in SALDI as compared to ligand-capped AuNP because the ligands can impede energy transfer to the analyte,[19,25] as they isolate the analyte from the AuNP. When the ligands were removed, analytes are closer to the nanoparticle surface and energy transfer is more effective, thus enhancing DIE.

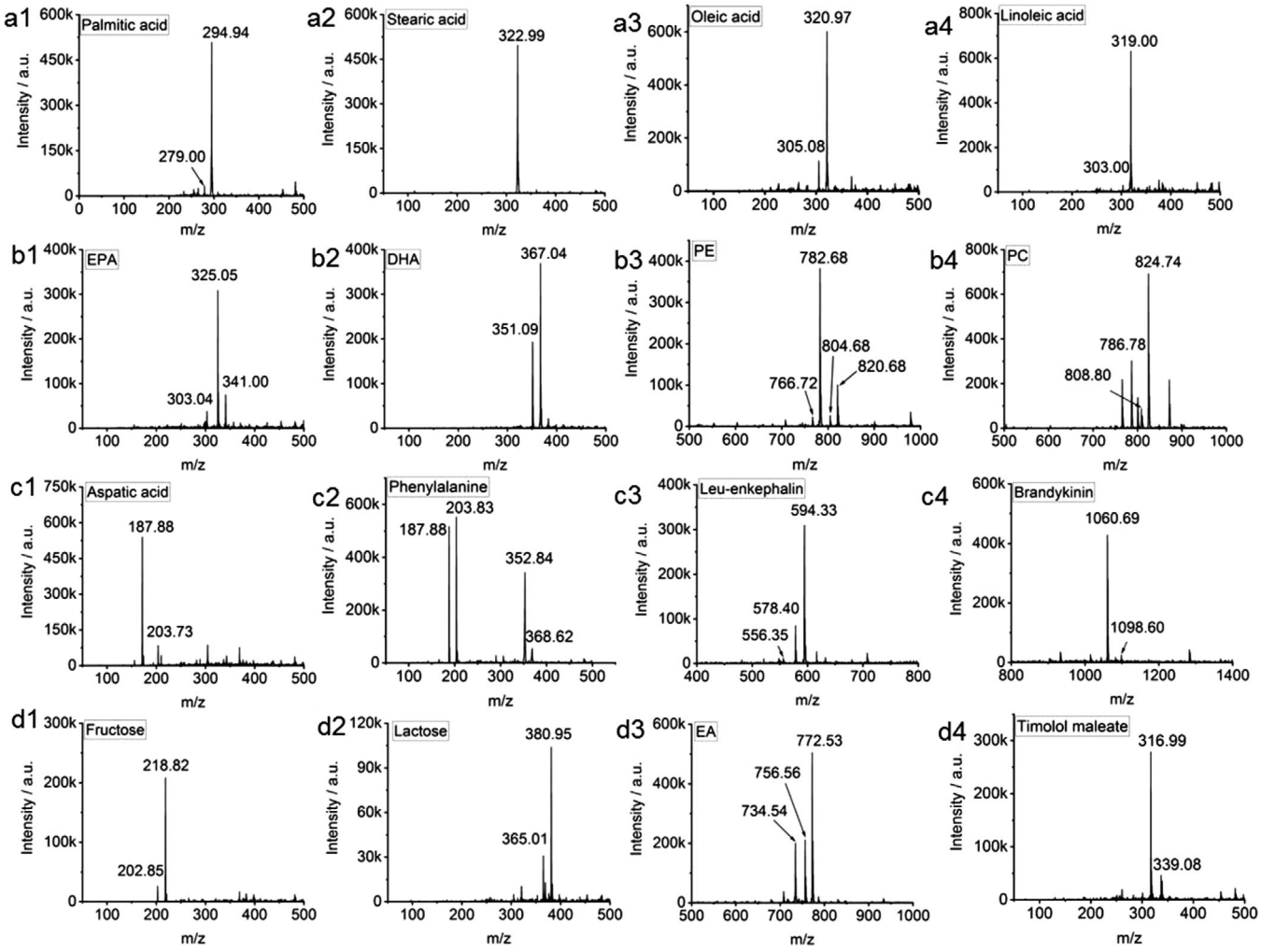

FIGURE 5 AuNP[H-4-H]-assisted LDI mass spectra of (a1-b2) fatty acids, (b3, b4) lipids, (c1, c2) amino acids, (c3, c4) peptides. and (d1, d2) saccharides, (d3, d4) drugs (concentration, 100 μM ea.)

An experiment was designed to investigate this effect for our AuNP, exemplified by AuNP[D-1-H]. In this experiment, the deposited AuNP were laser-irradiated prior to sample deposition, to remove the organic ligand as well as any impurities embedded in the AuNP or present on the metal target. Laser ablation is frequently used in analytical chemistry to remove small amounts of material from solids.[40] As previously reported for our experimental setup,[31] SALDI with laser powers $\leq$ 50% did not ablate gold from the substrate and consequently no gold-related ions were visible in the mass spectra under atmospheric pressure SALDI-MS conditions. For the cleaning step, different laser energies between 10% and 50% were investigated. For low energies (<30%), there was no noticeable ablation effect as no signals from ligands/impurities were visible in the mass spectra. For laser energies >30%, strong signals of ligands and other impurities started to appear, mainly in the *m/z* range of 200 to 450 for AuNP[D-1-H] substrates. A setting of 50% was chosen for efficient removal, which was the same energy used in the subsequent LDI experiments of the analyte (see Section 2).

The comparison between the regular experiments and those utilizing the additional laser ablation is illustrated in Figure 4 for different concentration levels of the AuNP. It is immediate obvious that the background noise levels were significantly reduced across the investigated *m/z* range, in particular at high AuNP concentrations, which strongly increased signal-to-noise ratios for linoleic acid. Moreover, ion currents of the analyte also strongly increased as compared to the ligand-capped AuNP, further amplifying the sensitivity gain. In fact, for the highest AuNP concentration, ion currents for linoleic were amplified almost 20-fold in comparison to the capped AuNP (along with the reduced noise levels!). This amplification factor was lower for lower concentrations of AuNP. We hypothesize that this was due to ablation losses of nanoparticles during the initial laser irradiation phase, which are expected to have a higher relative impact for low concentrations of AuNP, which will then result in reduced DIE (the numerical differences between capped versus irradiated nanoparticles are summarized in Figure S1). As noise levels were also reduced at lower nanoparticle concentrations for the capped AuNP (Figure 4), the overall gain of this procedure was not as important for low AuNP concentrations.

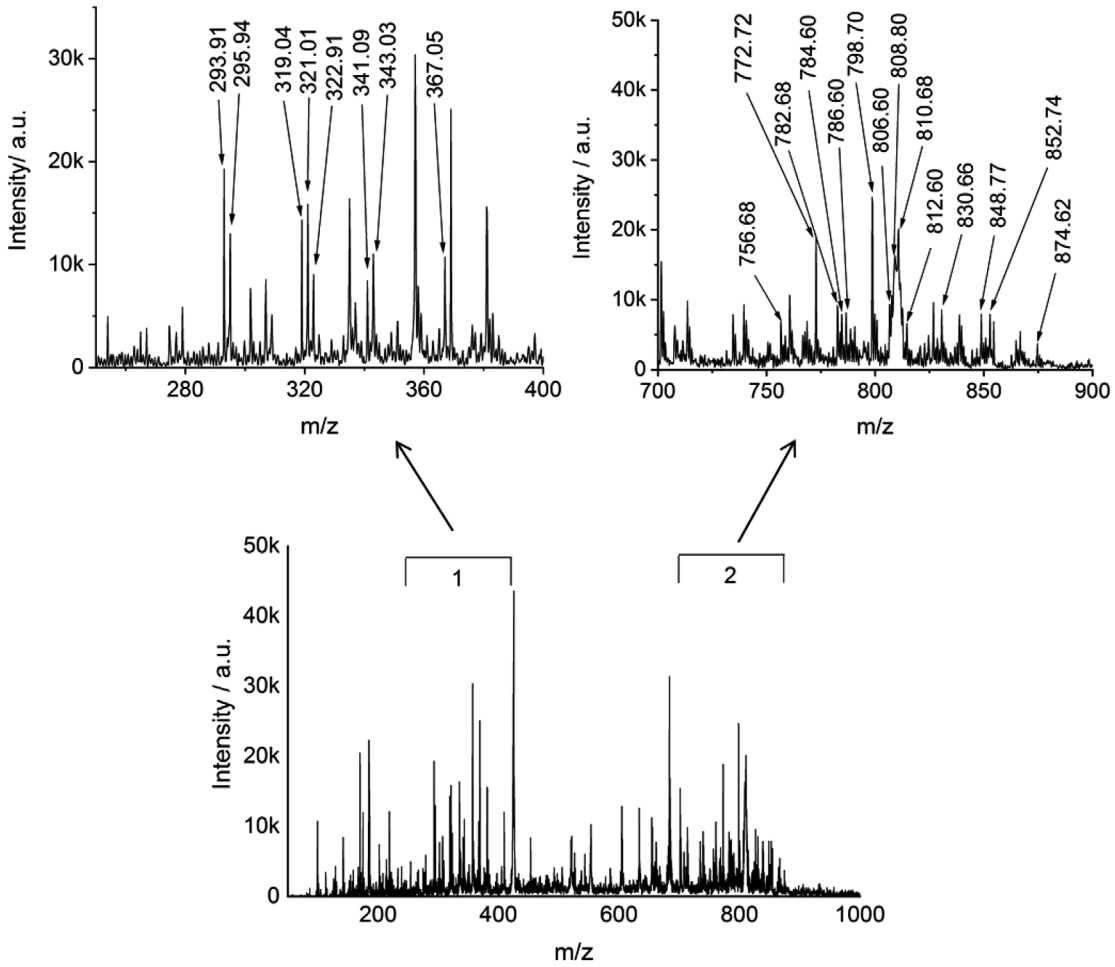

FIGURE 6 AuNP[H-4-H]-assisted LDI mass spectra of a crude pig brain extract (the brain extract was diluted 10-fold prior to analysis; tentative lipid assignments are labelled with corresponding *m/z* value)

3.2.4 | Nanoparticle core size

AuNP with radii of 1.2, 3.2, and 4.7 nm were used to study core size effects on DIE of linoleic acid. As seen in Figure 3C, the signal intensity for linoleic acid always increased in the order 4.7 > 3.2 > 1.2 nm particle size, regardless of the nature of the organic ligand attached to the AuNP. As shown by McLean *et al*,[24] the size of AuNP had a strong effect on signal intensity for angiotensin for gold nanoparticles in the range of 2-10 nm. Larger AuNP provided higher DIE in SALDI, although a strong noise background of gold ions was observed for the larger nanoparticles. In our experiments, no gold-related ions were seen in the mass spectra, even for larger nanoparticles. This is probably due to the softer nature of the AP-SALDI process in comparison to vacuum SALDI. As demonstrated in our previous work,[31] no gold-related ions were observed under atmospheric pressure for $[AuNP]_n$ substrates, whereas gold-related ions were clearly seen under vacuum SALDI conditions. Under atmospheric pressure SALDI, there was insufficient energy for ablation and ionization of gold ions and the local temperature rise on the target plate upon laser irradiation was likely not as high. For AuNP containing alkanethiol ligands, the signal intensity of linoleic acid from AuNP with radius of 4.8 nm was approximately twofold higher than for AuNP of radius 3.2 mm and ~4.8-fold higher for particles of 1.2 nm. AuNP with oleyamine exhibited the same trend; that is, signal intensity for radius of 4.8 nm was ~2.3× higher than for 3.2 mm, and 6.5× higher than for 1.2 mm. The size effect is probably related to the stronger UV/Vis absorption for larger nanoparticles than for smaller particles, allowing higher energy transfer from the larger nanoparticles to the analyte.

3.2.5 | Nanoparticle concentration

In order to investigate the influence of the concentration of the nanoparticle solution, the stock AuNP[D-1-H] solution (radius, 1.2 nm at 2 mg/mL) was diluted to give AuNP solutions of 1.0, 0.4, 0.2, 0.1, and 0.04 mg/mL, respectively, which were then deposited onto the SALDI targets (NB: AuNP solutions that were diluted more than 20 times were virtually without color). As shown in Figure 3D, the signal intensity of linoleic acid decreased

with decreasing AuNP concentration; for concentrations < 0.1 mg/mL, the signal intensity of linoleic acid stayed virtually the same. The signal intensity of linoleic acid from 2 mg/mL AuNP preparations was approximately 10-fold higher than for 0.2 mg/mL. As the number of ions formed during desorption/ionization is proportional to the amount of energy absorbed and transferred to the analytes,[41] the observed intensity decrease can be readily explained with decreased UV/Vis absorption of the AuNPs. For very small AuNP concentrations, with negligible UV/Vis absorption, we suggest that direct analyte LDI takes over as primary mechanism, which is not very efficient for the analyte linoleic acid, resulting in very low ion currents regardless of concentration.

3.3 | Application to wider range of biomolecules and brain extract

For application to other analytes, AuNP[H-4-H] was used as optimized material to analyze a wide range of biomolecules. Biomolecules including fatty acids (palmitic acid, stearic acid, oleic acid, linoleic acid), phospholipids (PE, PC), amino acids (aspartic acid, phenylalanine), small peptides (leu-enkephalin, bradykinin), saccharides (D-fructose, D-lactose) and drugs (erythromycin A, timolol maleate) were chosen for this application. Figure 5 illustrates that all investigated analytes were ionized intact without fragmentation. They were detected at limits of detection (LOD) of approximately 1 μM (Figure S2 illustrates the SALDI spectra at different concentrations down to the LOD; LOD was defined as the lowest concentration, for which a signal-to-noise ratio of at least 3:1 was obtained). Please note that while these LOD numbers appear relatively high, they are mainly the result of the used instrument, which was an insensitive, older generation 3D ion trap utilized for the proof-of-concept work described in this study. Transferring this technique to a modern triple quadrupole instrument with a high duty cycle data acquisition mode (such as single reaction monitoring, SRM), would lower LOD by at least 100-1000-fold as previously shown for quantitative MALDI analysis of small molecules.[42,43]

Finally, as further proof-of-concept, we applied our AuNP-assisted LDI technique to a very complex biological mixture; that is, a crude extract of a pig brain. After sample preparation (see Section 2), these extracts contain a large number of lipid species such as fatty acids, PC, PE, cerebrosides etc.[44,45] AuNP[H-4-H] was used as substrate in the analysis and we were able to detect a wide range of lipids, as shown in Figure 6 (suggested, tentative structural assignments, and the implemented identification procedure for fatty acids as well as PC and PE species in the *m/z* ranges of 200-400 and 700-900 are summarized in Table S1). Obviously, the implemented mass analyzer, which operated at nominal mass resolution, did not provide sufficient mass accuracy for elemental formulae assignments, but this information could be readily obtained by using a high resolution mass spectrometer for the experiments.

4 | CONCLUSIONS

A series of AuNP of different core size and capping ligands were prepared for SALDI-MS. AuNP were first characterized by SAXS and UV/Vis spectra, followed by SALDI-MS to optimize the performance and the DIE of the test analyte linoleic acid. The results showed that core size, capping ligands, and concentration of AuNP played important roles in the performance of the substrate. For AuNP with larger core sizes, high concentrations of hydrophobic ligands provided higher DIE of analytes. It was found that the surface chemistry of the AuNP had a stronger influence on the DIE than the UV/Vis absorption of the material. For similar surface chemistries, stronger UV/Vis absorption will further improve the performance. In a separate experiment, we demonstrated that laser pretreatment of the AuNP, to remove the organic ligands and embedded impurities, increased DIE approximately 20-fold for high concentrations of AuNP. This amplification was less pronounced for lower concentrations of the nanoparticles.

Under optimized condition, the AuNP were successfully used to analyze a wide arrange of different low molecular weight biomolecules. In addition, the analysis of a crude pig brain extract readily demonstrated the ability of the technique to detect a wide range of lipid species within a highly complex sample. In the future, we are planning to expand this study and conduct a comprehensive method validation for quantitative SALDI-MS analysis of selected analytes for application to various biological samples.

We believe that the SALDI-MS technique described here would be particularly useful as a method for quantitative analysis of small biological molecules but would equally well serve as a molecular weight readout platform for metabolome analyses if combined with high resolution mass spectrometry.

ACKNOWLEDGMENTS

The authors thank Dr. Ignacy Rzagalinski (Max-Planck Institute of Molecular Cell Biology and Genetics, Dresden) for providing the pig brain extracts and Caroline Hoffmann (Saarland University, Saarbrücken) for UV/Vis measurements. Z.L. acknowledges the China Scholarship Council for financial support.

CONFLICT OF INTEREST

D.A.V. is Editor-in-Chief of *Analytical Science Advances*.

DATA AVAILABILITY STATEMENT

The data that support the findings of this study are available from the corresponding author upon reasonable request.

REFERENCES

1. Tanaka K, Waki H, Ido Y, et al. Protein and polymer analyses up to m/z 100 000 by laser ionization time-of-flight mass spectrometry. *Rapid Commun Mass Spectrom*. 1988;2:151-153.
2. Cha S, Yeung ES. Colloidal graphite-assisted laser desorption/ionization mass spectrometry and MSn of small molecules. 1. Imaging of cerebrosides directly from rat brain tissue. *Anal Chem*. 2007;79:2373-2385.
3. Shi C, Deng C, Zhang X, Yang P. Synthesis of highly water-dispersible polydopamine-modified multiwalled carbon nanotubes for matrix-assisted laser desorption/ionization mass spectrometry analysis. *ACS Appl Mater Interfaces*. 2013;5:7770-7776.
4. Lin Z, Wu J, Dong Y, Xie P, Zhang Y, Cai Z. Nitrogen and sulfur co-doped carbon-dot-assisted laser desorption/ionization time-of-flight mass spectrometry imaging for profiling bisphenol S distribution in mouse tissues. *Anal Chem*. 2018;90:10872-10880.
5. Wei J, Buriak JM, Siuzdak G. Desorption–ionization mass spectrometry on porous silicon. *Nature*. 1999;399:243-246.
6. Yang H, Su R, Wishnok JS, et al. Magnetic silica nanoparticles for use in matrix-assisted laser desorption ionization mass spectrometry of labile biomolecules such as oligosaccharides, amino acids, peptides and nucleosides. *Microchim Acta*. 2019;186:104.
7. Amin MO, Al-Hetlani E. Tailoring the surface chemistry of SiO_2-based monoliths to enhance the selectivity of SALDI-MS analysis of small molecules. *Talanta*. 2019;200:458-467.
8. Silina YE, Koch M, Volmer DA. The Role of Physical and chemical properties of Pd nanostructured materials immobilized on inorganic carriers on ion formation in atmospheric pressure laser desorption/ionization mass spectrometry. *J Mass Spectrom*. 2014;49:468-480.
9. Ding F, Qian Y, Deng Z, et al. Size-selected silver nanoparticles for MALDI-TOF mass spectrometry of amyloid-beta peptides. *Nanoscale*. 2018;10:22044-22054.
10. Silina YE, Meier F, Nebolsin VA, Koch M, Volmer DA. Novel galvanic nanostructures of Ag and Pd for efficient laser desorption/ionization of low molecular weight compounds. *J Am Soc Mass Spectrom*. 2014;25:841-851.
11. Kim M, Park JM, Yun TG, Noh JY, Kang MJ, Pyun JC. TiO2 nanowires from wet-corrosion synthesis for peptide sequencing using laser desorption/ionization time-of-flight mass spectrometry. *ACS Appl Mater Interfaces*. 2018;10:33790-33802.
12. Yan B, Jeong Y, Mercante LA, et al. Characterization of surface ligands on functionalized magnetic nanoparticles using laser desorption/ionization mass spectrometry (LDI-MS). *Nanoscale*. 2013;5:5063-5066.
13. Kim K, Um K, Yoon C, Ryoo WS, Lee K. Wafer-level detection of organic contamination by ZnO-rGO hybrid-assisted laser desorption/ionization time-of-flight mass spectrometry. *Talanta*. 2018;182:273-278.
14. Coffinier Y, Szunerits S, Drobecq H, Melnyk O, Boukherroub R. Diamond nanowires for highly sensitive matrix-free mass spectrometry analysis of small molecules. *Nanoscale*. 2012;4:231-238.
15. Lu T, Olesik SV. Electrospun nanofibers as substrates for surface-assisted laser desorption/ionization and matrix-enhanced surface-assisted laser desorption/ionization mass spectrometry. *Anal Chem*. 2013;85:4384-4391.
16. Kim YK, Wang LS, Landis R, Kim CS, Vachet RW, Rotello VM. A layer-by-layer assembled MoS_2 thin film as an efficient platform for laser desorption/ionization mass spectrometry analysis of small molecules. *Nanoscale*. 2017;9:10854-10860.
17. Wang H, Wu Y, Guo B, Sun W, Ding L, Chen B. Quantification of low-polar small molecules using room temperature ionic liquids matrix-assisted desorption corona beam ionization. *Analyst*. 2012;137:3982-3988.
18. Chiang CK, Chen WT, Chang HT. Nanoparticle-based mass spectrometry for the analysis of biomolecules. *Chem Soc Rev*. 2011;40:1269-1281.
19. Mandal A, Singha M, Addy PS, Basak A. Laser desorption ionization mass spectrometry: recent progress in matrix-free and label-assisted techniques. *Mass Spectrom Rev*. 2019;38:3-21.
20. Silina YE, Volmer DA. Nanostructured solid substrates for efficient laser desorption/ionization mass spectrometry (LDI-MS) of low molecular weight compounds. *Analyst*. 2013;138:7053-7065.
21. Unnikrishnan B, Chang CY, Chu HW, Anand A, Huang CC. Functional gold nanoparticles coupled with laser desorption ionization mass spectrometry for bioanalysis. *Anal Methods*. 2016;8:8123-8133.
22. Pilolli R, Palmisano F, Cioffi N. Gold nanomaterials as a new tool for bioanalytical applications of laser desorption ionization mass spectrometry. *Anal Bioanal Chem*. 2012;402:601-623.
23. Abdelhamid HN, Wu HF. Gold nanoparticles assisted laser desorption/ionization mass spectrometry and applications: from simple molecules to intact cells. *Anal Bioanal Chem*. 2016;408:4485-4502.
24. McLean JA, Stumpo KA, Russel DH. Size-selected (2-10 nm) gold nanoparticles for matrix assisted laser desorption ionization of peptides. *J Am Chem Soc*. 2005;127:5304-5305.
25. Amendola V, Litti L, Meneghetti M. LDI-MS assisted by chemical-free gold nanoparticles: enhanced sensitivity and reduced background in the low-mass region. *Anal Chem*. 2013;85:11747-11754.
26. Kolářová L, Kučera L, Vaňhara P, Hampl A, Havel J. Use of flower-like gold nanoparticles in time-of-flight mass spectrometry. *Rapid Commun Mass Spectrom*. 2015;29:1585-1595.
27. Castellana ET, Gamez RC, Gómez ME, Russell DH. Longitudinal surface plasmon resonance based gold nanorod biosensors for mass spectrometry. *Langmuir*. 2010;26:6066-6070.
28. Palermo A, Forsberg EM, Warth B, et al. Fluorinated gold nanoparticles for nanostructure imaging mass spectrometry. *ACS Nano*. 2018;12:6938-6948.
29. Chiang NC, Chiang CK, Lin ZH, Chlu TC, Chang HT. Detection of aminothiols through surface-assisted laser desorption/ionization mass spectrometry using mixed gold nanoparticles. *Rapid Commun. Mass Spectrom*. 2009;23:3063-3068.
30. Son J, Lee G, Cha S. Direct analysis of triacylglycerols from crude lipid mixtures by gold nanoparticle-assisted laser desorption/ionization mass spectrometry. *J Am Soc Mass Spectrom*. 2014;25:891-894.
31. Liu Z, Zhang P, Kister T, Kraus T, Volmer DA. Ultra-thin homogenous AuNP monolayers as tunable functional substrates for surface-assisted laser desorption/ionization of small biomolecules. *J Am Soc Mass Spectrom*. 2020;21:47-57.

32. Tang HW, Lu W, Che CM, Ng KM. Gold nanoparticles and imaging mass spectrometry: double imaging of latent fingerprints. *Anal Chem*. 2010;82:1589-1593.
33. Want EJ, Masson P, Michopoulos F, et al. Global metabolic profiling of animal and human tissues via UPLC-MS. *Nat Protoc*. 2013;8:17-32.
34. Wu BH, Yang HY, Huang HQ, Chen GX, Zheng NF. Solvent effect on the synthesis of monodisperse amine-capped Au nanoparticles. *Chinese Chem Lett*. 2013;24:457-462.
35. Kister T, Maurer JHM, González-García L, Kraus T. Ligand-dependent nanoparticle assembly and its impact on the printing of transparent electrodes. *ACS Appl Mater Interfaces*. 2018;10:6079-6083.
36. Laiko VV, Moyer SC, Cotter RJ. Atmospheric pressure MALDI/Ion trap mass spectrometry. *Anal Chem*. 2000;72:5239-5243.
37. Keller C, Maeda J, Jayaraman D, et al. Comparison of vacuum MALDI and AP-MALDI platforms for the mass spectrometry imaging of metabolites involved in salt stress in medicago truncatula. *Front Plant Sci*. 2018;9:1238.
38. Miller CA, Yi D, Perkins PD. An atmospheric pressure matrix-assisted laser desorption/ionization ion trap with enhanced sensitivity. *Rapid Commun Mass Spectrom*. 2003;17:860-868.
39. Tan PV, Laiko VV, Doroshenko VM. Atmospheric Pressure MALDI with pulsed dynamic focusing for high-efficiency transmission of ions into a mass spectrometer. *Anal Chem*. 2004;76:2462-2469.
40. Russo RE, Mao X, Liu H, Gonzalez J, Mao SS. Laser ablation in analytical chemistry—a review. *Talanta*. 2002;57:425-451.
41. Luo G, Marginean I, Vertes A. Internal energy of ions generated by matrix-assisted laser desorption/ionization. *Anal Chem*. 2002;74:6185-6190.
42. Volmer DA, Sleno L, Bateman K, et al. Comparison of MALDI to ESI on a triple quadrupole platform for pharmacokinetic analyses. *Anal Chem*. 2007;79:9000-9006.
43. Sleno L, Volmer DA. Toxin screening in phytoplankton: detection and quantitation using MALDI triple quadrupole mass spectrometry. *Anal Chem*. 2005;77:1509-1517.
44. Gode D, Volmer DA. Lipid imaging by mass spectrometry-a review. *Analyst*. 2013;138:1289-1315.
45. Cha S, Yeung ES. Colloidal graphite-assisted laser desorption/ionization mass spectrometry and MSn of small molecules. 1. Imaging of cerebrosides directly from rat brain tissue. *Anal Chem*. 2007;79:2373-2385.

SUPPORTING INFORMATION

Additional supporting information may be found online in the Supporting Information section at the end of the article.

How to cite this article: Liu Z, Zhang P, Pyttlik A, Kraus T, Volmer DA. Influence of core size and capping ligand of gold nanoparticles on the desorption/ionization efficiency of small biomolecules in AP-SALDI-MS. *Anal Sci Adv*. 2020;1:210–220.
https://doi.org/10.1002/ansa.202000002